Journal of Magnetic Resonance 200 (2009) 280–284

Contents lists available at ScienceDirect

Journal of Magnetic Resonance

journal homepage: www.elsevier.com/locate/jmr

Proton NMR studies of the $NaAlH_4$ structure

L.E. Valiente-Banuet [a], G. Majer [a,*], K. Müller [b,c,d,*]

[a] Max-Planck-Institut für Metallforschung, Heisenbergstr. 3, D-70569 Stuttgart, Germany
[b] Institut für Physikalische Chemie, Universität Stuttgart, Pfaffenwaldring 55, D-70569 Stuttgart, Germany
[c] Dipartimento di Ingegneria dei Materiali e Tecnologie Industriali, Universitá degli Studi di Trento, via Mesiano 77, I-38100 Trento, Italy
[d] INSTM, UdR Trento, Italy

ARTICLE INFO

Article history:
Received 17 March 2009
Revised 9 July 2009
Available online 14 July 2009

Keywords:
NMR
Magic echo
Second moment
Structure determination
Chemical hydride
Sodium alanate
Hydrogen storage

ABSTRACT

Advanced nuclear magnetic resonance (NMR) techniques were applied to study the local environments of hydrogen in $NaAlH_4$. Through a combined application of the magic echo (ME) and the magic Hahn echo (MHE) sequences the hetero- and homonuclear contributions to the dipolar second moment (M_2) were determined separately. The obtained values are compared with the second moments calculated by the van Vleck formulae, using structural data determined by neutron scattering on $NaAlD_4$. This comparison indicates structural differences between $NaAlH_4$ and $NaAlD_4$. A model is suggested for the orientation of the $[AlH_4]^-$ tetrahedra in $NaAlH_4$, for which the calculated second moments are in good agreement with the experimentally observed values.

1. Introduction

Complex hydrides can release hydrogen through chemical decomposition reactions and are thus of great interest as potential hydrogen storage materials. A particularly promising candidate for the development of a reversible hydrogen storage system is metal doped sodium alanate $NaAlH_4$. It decomposes in two steps, first into the hexahydride Na_3AlH_6, which further decomposes into NaH as follows

$$NaAlH_4 \leftrightarrow \frac{1}{3}Na_3AlH_6 + \frac{2}{3}Al + H_2 \quad (1)$$

$$\frac{1}{3}Na_3AlH_6 \leftrightarrow NaH + \frac{1}{3}Al + \frac{1}{2}H_2 \quad (2)$$

The first reaction step releases 3.7 wt% H_2 and the second step 1.9 wt% H_2, resulting in a total of 5.6 wt% reversible hydrogen storage. Since the discovery by Bogdanović and Schwickardi [1], that the inverse of reactions (1) and (2) can be catalyzed by the addition of a small amount of Ti-based complexes, the interest in $NaAlH_4$ for hydrogen storage increased strongly. The admixture of a few mole percent of Ti-based catalysts enhances both de- and rehydrogenation rates, and it reduces the dehydriding temperature of $NaAlH_4$ considerably [1]. The catalyst can be incorporated into $NaAlH_4$ either by chemical solution processes [1,2] or simply by adding the catalyst precursor to the alanate and ball milling the mixture under inert gas atmosphere [3,4]. Suitable catalyst precursors are Ti^{3+} cations in the form of chlorides [5–7] or small Ti_{13}-clusters [8,9]; the latter considered to hold the highest potential for rapid release and absorption of hydrogen gas.

Early single crystal X-ray diffraction studies [10,11] have shown that $NaAlH_4$ has a body-centered tetragonal unit cell with the space group $I4_1/a$. However, as Bel'skii et al. [11] pointed out, X-ray diffraction data give very large uncertainties in the hydrogen coordinates. In order to obtain the correct location of the hydrogen/deuterium atoms, Hauback et al. [12] determined the structure of $NaAlD_4$ from Rietveld-type refinements of powder neutron diffraction data. These studies confirmed the space group $I4_1/a$ and yielded the lattice parameters $a = 5.0119$ and $c = 11.3147$ Å at 295 K [12]. The lattice parameters for Ti-doped $NaAlD_4$ [13] are found to be within 0.1% of the values for undoped $NaAlD_4$ observed by Hauback et al. [12]. X-ray diffraction studies on $NaAlH_4$ also indicate that there is no significant variation of the lattice parameter if the material is doped with Ti_{13}-clusters [14]. A detailed knowledge of the crystal structure of $NaAlH_4$, in particular the coordinates for hydrogen, is necessary to understand the processes occurring in the material during the decomposition processes (1) and (2).

Nuclear magnetic resonance (NMR) spectroscopy is a powerful tool to study structural and dynamical properties of solids. However, only few NMR studies have been performed so far on complex chemical hydrides. The first ^1H NMR investigations of hydrogen

* Corresponding authors. Fax: +49 711 689 3612 (G. Majer); +39 0461 882439 (K. Müller).
E-mail addresses: majer@mf.mpg.de (G. Majer), k.mueller@ipc.uni-stuttgart.de, klaus.mueller@ing.unitn.it (K. Müller).

1090-7807/$ - see front matter © 2009 Elsevier Inc. All rights reserved.
doi:10.1016/j.jmr.2009.07.011

dynamics in the hexahydride Na_3AlH_6 were performed in 1981 by Senegas et al. [15]. Measurements of the ^2H, ^{23}Na, and ^{27}Al quadrupole coupling constants have been performed on $NaAlH_4$ and its isotopic modification $NaAlD_4$ [16]. The Ti-catalyzed thermal decomposition of $LiAlH_4$ has been studied by ^{27}Al magic angle spinning (MAS) NMR spectroscopy [17,18]. The effects of Ti-based catalysts on the dehydriding of sodium alanates $NaAlH_4$ and Na_3AlH_6 have been monitored by proton NMR spectroscopy [19]. The hydrogen discharging and recharging process of Ti-doped $NaAlH_4$ has also been investigated by ^{27}Al [20,21], ^{23}Na [20] and ^1H MAS NMR spectroscopy [21].

In $NaAlH_4$ samples with a very high purity no motion-induced dipolar relaxation occurs and the impurity-related paramagnetic relaxation is also very slow. Thus, long spin–lattice relaxation times T_1 with values up to 1 h have been observed in pure $NaAlH_4$ at room temperature [19]. Such long T_1 values make NMR measurements extremely time consuming. In the Ti-doped samples of the present work, the nuclear magnetization recovers much faster with relaxation times in the range of a few minutes. This allowed us to perform the NMR measurements within a reasonable time.

The present paper aims for the first time at a precise determination of the positions of the hydrogen atoms in $NaAlH_4$ by means of solid-state NMR spectroscopy. Special emphasis is put on NMR pulse sequences which generate spin echoes for solids with a strong dipolar coupling in the rigid-lattice regime. In particular, the magic echo (ME) and magic Hahn echo (MHE) sequences are applied to measure the second moment of the dipolar interactions in $NaAlH_4$. The different contributions to the second moment depend on the interatomic distances between hydrogen atoms or between a given hydrogen atom and the different types of neighboring atoms.

2. Magic echoes

For solids with a strong dipolar coupling in the rigid-lattice regime, i.e., at a temperature well below the onset of motional narrowing, the time-domain free induction decay (FID) of the NMR signal is well represented by

$$G_{\mathrm{FID}}(t) = G_0 \exp\left(-\frac{M_2}{2}t^2\right) \tag{3}$$

The second moment M_2 in Eq. (3) is usually given by the sum of two contributions

$$M_2 = M_{2,\mathrm{homo}} + M_{2,\mathrm{hetero}} \tag{4}$$

which are due to homonuclear and heteronuclear dipolar coupling, respectively. For protons in a specific site, these contributions can be calculated according to the van Vleck formulae [22]

$$M_{2,\mathrm{homo}} = \frac{3}{5}\gamma_I^4\hbar^2 I(I+1)\sum_j \frac{1}{r_{ij}^6} \tag{5}$$

and

$$M_{2,\mathrm{hetero}} = \frac{4}{15}\gamma_I^2\gamma_S^2\hbar^2 S(S+1)\sum_j \frac{1}{r_{ij}^6} \tag{6}$$

where the summation in Eq. (5) runs over the distances to all other protons, and the summation in Eq. (6) runs over the distances to all heteronuclei (e.g., ^{23}Na and ^{27}Al). Here, I, γ_I, S, and γ_S are the spin and gyromagnetic ratios of the proton and the other kind of nuclei, respectively.

Dipolar NMR lineshapes have been widely used to determine and to clarify the structures of solids. Such structure determinations from NMR lineshapes are usually performed by comparing the experimental second moment M_2 with calculated values. However, the initial part of $G(t)$, which makes the most important contribution to M_2, is usually hidden by the recovery of the probe and receiver circuits from the r.f. pulse overload. This experimental dead time is typically of the order of a few microseconds. Hence, an accurate determination of M_2 from the FID following a single $\pi/2$-pulse becomes more difficult as M_2 increases.

The use of magic echo pulse sequences [23–27] permits to overcome the recovery time difficulties by generating well-defined echoes with minimal lineshape distortion. These sequences produce coherence evolution conditions in subsequent intervals so that the sign of the interaction Hamiltonian is reversed. Rather complex multiple-pulse sequences were originally utilized to produce the magic echoes [23–27]. Simplified versions of the magic echo sequence were applied to obtain accurate M_2 values for polycrystalline dihydrides $TiH_{1.98}$ [28] and trihydrides YH_3 and LuH_3 [29].

The magic echo (ME) and magic Hahn echo (MHE) pulse sequences used in the present work are shown in Fig. 1. The magic echo uses on-resonance r.f. pulses to effectively time-reverse the system evolution under the like-spin dipolar interaction. First, a $(\pi/2)$ r.f. pulse is applied along the x axis of the rotating frame which excites coherence evolving during an interval τ prior to the "magic sandwich" pulse. During the magic sandwich pulse the like-spin dipolar Hamiltonian is $-1/2$ times the dipolar Hamiltonian in the absence of r.f. irradiation. For magic sandwich duration of 4τ, the magic echo appears after another free-evolution interval of length τ [30–32]. The echo maximum representing the completely refocused coherence is thus reached after a total time of 6τ, whereas the effective time for spin evolution is 4τ due to the reduced Hamiltonian during the magic sandwich pulse. This ME pulse sequence selectively recovers spin coherence which has been defocused by homonuclear spin interactions. However, heteronuclear spin couplings are not compensated. With the classical two-pulse echo by Hahn [33] the situation is reversed. This pulse sequence fails to refocus dephasing by homonuclear spin interactions, whereas those caused by heteronuclear spin couplings are compensated for. To combine the ME and the Hahn pulse sequences, a π-pulse is inserted in the ME sequence simply by inverting the phase of the $(\pi/2)$ r.f. pulse after the magic sandwich [31,32,34].

With the MHE sequence the nuclear magnetization is almost entirely restored, and any decay of $G_{\mathrm{MHE}}(\tau)$ with increasing τ is due to experimental imperfections such as incomplete cancelling of the r.f. irradiations along the x and $-x$ directions in the rotating frame. The FID signal $G_{\mathrm{FID}}(t)$ can be deduced from the second half of the MHE without having any distortions due to an experimental dead time. $G_{\mathrm{FID}}(t)$ decays with time due to both homonuclear and heteronuclear interactions. Thus, the dependence of $G_{\mathrm{FID}}(t)$ on the spin-evolution time t, normalized to $G_{\mathrm{MHE}}(t)$, makes it possible to determine the sum of $M_{2,\mathrm{homo}}$ and $M_{2,\mathrm{hetero}}$ according to

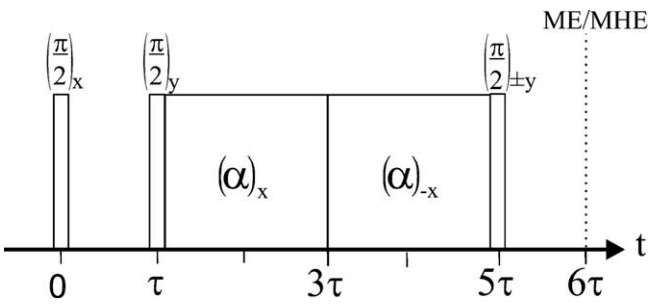

Fig. 1. Pulse sequences for the formation of a magic echo (ME) and a magic Hahn echo (MHE) [30]. The time reversal is provided by the "magic sandwich" pulse applied in the interval between the times $t = \tau$ and $t = 5\tau$. The ME is refocusing phase shifts due to homonuclear dipolar spin interactions but not those due to heteronuclear spin couplings. The MHE differs from the ME only by the phase of the r.f. pulse after the magic sandwich, which is then $-y$ instead of y. In this case both the homonuclear and the heteronuclear dipolar interactions are refocused.

$$\frac{G_{\mathrm{FID}}(t)}{G_{\mathrm{MHE}}(t)} = \exp\left(-\frac{M_{2,\mathrm{homo}} + M_{2,\mathrm{hetero}}}{2}t^2\right) \quad (7)$$

Accordingly, the variation of the amplitude of the magic echo $G_{\mathrm{ME}}(t)$ with the effective time for spin evolution under heteronuclear dipolar interaction, $t = 4\tau$, yields $M_{2,\mathrm{hetero}}$ by using the relation

$$\frac{G_{\mathrm{ME}}(t)}{G_{\mathrm{MHE}}(t)} = \exp\left(-\frac{M_{2,\mathrm{hetero}}}{2}t^2\right) \quad (8)$$

3. Experimental details

$NaAlH_4$ material was purchased as powder (Chemetall, Frankfurt) and purified by a Soxhlet extraction with tetrahydrofuran (THF) as described in [9]. To prevent moisture and oxygen from reacting with the material it was always handled in a glove box filled with purified argon. Ti-doped samples were prepared by ball milling of $NaAlH_4$ with 2.0 mol% of Ti_{13}·6THF under argon atmosphere with a Fritsch P6 planetary mill at 600 rotations per minute. The mechanical milling was done for two times 15 min with a 10 min break in between by using milling vial and balls of silicon nitride.

The NMR measurements were performed under static conditions with a Bruker CXP 300 spectrometer, operating at a proton resonance frequency of 300 MHz, which was equipped with a Tecmag control unit. The various experiments were done using a 5 mm Bruker double-resonance wideline probe. The $\pi/2$-pulse length was 2.7 μs, and the length of the time-reversal pulses τ in the magic echo (ME) and magic Hahn echo (MHE) sequences was varied between 2.5 and 50 μs. To improve the signal-to-noise ratio 4 scans were accumulated for each τ value. The delay between scans was 120 s to assure a complete recovery of the nuclear magnetization. All NMR measurements were done under N_2-atmosphere. The NMR spectra were obtained by Fourier transformation of the second half of the MHE, after multiplying the time-domain data by an apodizing function. The onset of the apodization was at a decay time of 25 μs, at which the FID was about 3% of its starting value.

To minimize the fraction of material which had already decomposed into Na_3AlH_6, the NMR measurements were always performed on freshly prepared samples. Nevertheless, it cannot be excluded that small amounts of Na_3AlH_6 were already present in the samples after the ball milling. Any traces of Na_3AlH_6 contribute to the NMR signal with a long tail in the FID [19], which is, however, completely suppressed by the apodization.

4. Results and discussion

The room-temperature proton NMR spectrum of $NaAlH_4$ is shown in Fig. 2. It consists of a single line which is roughly 45 kHz wide. Between 295 K and 130 K no significant change in the width or shape of the NMR line was observed. This indicates that the rigid lattice condition is already fulfilled at room temperature.

In order to gain structural information on $NaAlH_4$, the different contributions to the dipolar second moment M_2 have been deduced from the magic echo data. A comparison of the room-temperature decay of the FID, the ME, and the MHE is given in Fig. 3. The most rapid decay was observed in the case of the FID, where dephasing occurs due to both homonuclear and heteronuclear dipolar interactions. Up to an evolution time of about 20 μs, the FID is well described by a Gaussian curve, as indicated by the dash-dotted line in Fig. 3. However, the magnetization does not simply decay to zero with time, but oscillates slightly. Such a Lowe beat in the FID has been observed before in the case of ^{19}F NMR on CaF_2 [35] and ^1H NMR on YH_3 [29]. The amplitudes of the ME and MHE have been obtained by Fourier transformation of the echoes and integrating over the spectra in the frequency domain. The decay of the ME amplitude, represented by the dashed line in Fig. 3, is slower than that of the FID due to refocusing of homonuclear dipolar interactions. Finally, in the case of the MHE sequence, a weak dependence of the echo amplitude on the spin-evolution time is expected, since both homonuclear and heteronuclear dipolar interactions should be refocused. As the solid line in Fig. 3 indicates, the amplitude of the MHE decreases indeed only very weakly with time according to $G_{\mathrm{MHE}}(t) = G_0 \exp\left(-\frac{\varepsilon}{2} \times t^2\right)$ with $\varepsilon = 2.5 \times 10^8\ \mathrm{Hz}^2$.

Eq. (7) allows us now to determine M_2, the sum of $M_{2,\mathrm{homo}}$ and $M_{2,\mathrm{hetero}}$, from the decay rates of $G_{\mathrm{FID}}(t)$ and $G_{\mathrm{MHE}}(t)$ which was found to $M_2 = (140 \pm 2) \times 10^8\ \mathrm{Hz}^2$. The value $M_{2,\mathrm{hetero}} = (61 \pm 11) \times 10^8\ \mathrm{Hz}^2$ was obtained from an analysis of $G_{\mathrm{ME}}(t)$ and $G_{\mathrm{MHE}}(t)$ by using Eq. (8). With these two results, the value of $M_{2,\mathrm{homo}} = (79 \pm 13) \times 10^8\ \mathrm{Hz}^2$ was calculated by applying Eq. (4).

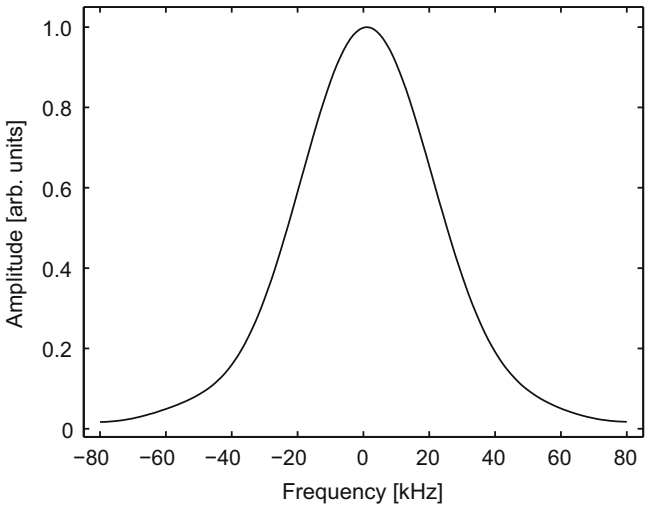

Fig. 2. Room-temperature proton NMR spectrum of $NaAlH_4$ obtained by Fourier transformation of the second half of the magic Hahn echo (MHE) measured at 300 MHz.

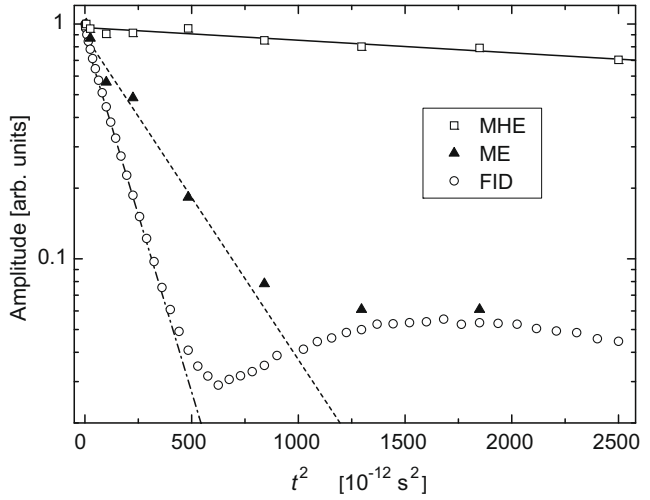

Fig. 3. Time evolution of NMR signals $G(t)$ plotted as a function of t^2. The circles represent the time development of the second half of the magic Hahn echo, which decays due to both homo- and heteronuclear dipolar interactions. The triangles and squares show the decay of the amplitude of the ME and the MHE, respectively. Here, the time *t denotes 4 times the* τ values indicated in Fig. 1, which is the effective time for spin evolution under dipolar interaction. The fitting curves were used to determine $M_{2,\mathrm{homo}}$ and $M_{2,\mathrm{hetero}}$.

Table 1
Experimental values of the homo- and heteronuclear contribution to the second moment in comparison with M_2 values calculated for different structures by using the van Vleck formulae [22].

	$M_{2,\text{total}}$ [10^8 Hz^2]	$M_{2,\text{homo}}$ [10^8 Hz^2]	$M_{2,\text{hetero}}$ [10^8 Hz^2]	$\Delta\nu$[1] [kHz]
Experimental values:	140 ± 2	79 ± 13	61 ± 11	44.3 ± 1.0
Calculations:				
0° configuration[2]	124.9	69.2	55.7	41.9
9° configuration[3]	135.6	79.5	56.1	43.6
10° configuration[3]	137.8	81.6	56.2	44.0
11° configuration[3]	140.4	84.2	56.2	44.4

[1] The linewidth $\Delta\nu$ is determined from the M_2 values (Eq. (9)).
[2] The 0° configuration refers to the structure reported in the literature for $NaAlD_4$ [12,13].
[3] The 9°, 10° and 11° configurations differ from the 0° configuration by the orientation of the $[AlH_4]^-$ tetrahedra. In these configurations it is assumed that the $[AlH_4]^-$ tetrahedra are rotated by 9°, 10° and 11°, respectively (for details see text).

Whereas M_2 could be determined very precisely, the experimental uncertainty in $M_{2,\text{hetero}}$ is somewhat larger, which also affects the accuracy in the determination of $M_{2,\text{homo}}$. The derived values are summarized in Table 1 together with the linewidth

$$\Delta\nu = \frac{\sqrt{M_2 2\ln(2)}}{\pi} \tag{9}$$

calculated from M_2 under the assumption of a Gaussian line shape.

For comparison with the experimental results we calculated second moments by using the van Vleck formulae for $M_{2,\text{homo}}$ and $M_{2,\text{hetero}}$. These calculations were first performed for the structure of $NaAlD_4$ reported in the literature [12,13]. The $NaAlD_4$ structure consists of isolated $[AlD_4]^-$ tetrahedra connected via Na^+ ions. Each $[AlD_4]^-$ tetrahedron is oriented such that all four faces are parallel to the faces of neighboring tetrahedra. This relative orientation is maintained if each tetrahedron is individually rotated by the same angle around its twofold symmetry axis parallel to the *c*-axis of the unit cell. This rotational degree of freedom is removed if, according to [12], the rotational orientation of the $[AlD_4]^-$ tetrahedra is such that the distance between adjacent deuterons on neighboring tetrahedra is maximized. In the following we denote this structure as the 0° configuration.

Ab initio calculations of the lattice parameters based on a generalized gradient approximation (GGA) are in good agreement with the data obtained by Rietveld refinement of X-ray and neutron diffraction data [13]. The GGA calculations yielded 1.631 Å for the Al–D bond length and 2.631 Å for the D–D distance within a tetrahedron. The corresponding value of the shortest distance between two deuterons on adjacent tetrahedra is 2.680 Å [13].

The numerical results of the GGA calculations [13] were used to compute the second moments. The summation in Eq. (5) was made over all protons up to a distance of 8.0 Å from a given proton. In the case of Eq. (6), all ^{23}Na and ^{27}Al nuclei within the same radius of 8.0 Å from a given proton were taken into account. The contributions of nuclei at a larger distance were estimated to be less than 1% of the calculated values. The obtained values of the second moments for the 0° configuration and the corresponding linewidth are also given in Table 1. The M_2 value for the 0° configuration is smaller than the experimentally observed second moment, which is an indication of structural differences between $NaAlH_4$ and its isotopic modification $NaAlD_4$. It is interesting to note that previous investigations of the ^{23}Na and ^{27}Al quadrupole coupling constants also yielded different values for $NaAlH_4$ and $NaAlD_4$ [16]. On the other hand, the heteronuclear contribution $M_{2,\text{hetero}}$ agrees within the experimental uncertainty with the measured value. This implies that the Al–H bond length and thus the size of the $[AlH_4]^-$ tetrahedra are as expected for the 0° structure. The difference in M_2 is only due to the difference in $M_{2,\text{homo}}$, which indicates that the homonuclear dipolar interaction in $NaAlH_4$ is in fact stronger than predicted for the 0° structure. It is reasonable to assume that the orientation of the $[AlH_4]^-$ tetrahedra in $NaAlH_4$ is different from that of the $[AlD_4]^-$ groups in $NaAlD_4$. One may think of a structure in which each $[AlH_4]^-$ tetrahedron is rotated by the same angle around its twofold symmetry axis parallel to the *c*-axis of the unit cell. If the tetrahedra are rotated by 9°, 10° and 11° the shortest distance between two protons on adjacent tetrahedra is reduced to 2.29 Å, 2.25 Å and 2.20 Å, respectively. The second moment values calculated for these configurations are included in Table 1. The calculated values of $M_{2,\text{hetero}}$ are only slightly changed compared to that of the 0° configuration, whereas the $M_{2,\text{homo}}$ values are considerably larger. Comparison of the values of $M_{2,\text{homo}}$ and M_2 calculated for, e.g., the 10° configuration with the measured values from our experiments shows good agreement in both cases. Thus, we suppose that the $[AlH_4]^-$ groups in $NaAlH_4$ are, indeed, rotated by about 10° compared to the situation in $NaAlD_4$. Nevertheless, other structural differences between $NaAlH_4$ and $NaAlD_4$ cannot be excluded.

Having a system in which D and H atoms occupy different sites is not unusual. A similar behavior has been observed previously in classical interstitial hydrides. A prominent example of that is the vanadium–hydrogen system, in which the different site occupancy results in different phase diagrams for the V–H and V–D systems [36].

5. Summary and conclusions

The present paper reports the first determination of the proton second moments of $NaAlH_4$ by applying the Magic Echo and Magic Hahn Echo sequences. By a combined analysis of the results obtained with both sequences, the contributions due to the homonuclear and the heteronuclear spin interactions could be separated. From a comparison with calculated second moments we conclude that structural differences between $NaAlH_4$ and $NaAlD_4$ exist. We propose that all $[AlH_4]^-$ tetrahedra in $NaAlH_4$ are rotated by about 10° around their twofold symmetry axes parallel to the *c*-axis of the unit cell, resulting in a distance of about 2.25 Å between closest hydrogen atoms on two adjacent tetrahedra. This rather simple model is capable of describing the experimental data consistently.

Acknowledgments

This work has been supported by the Deutsche Forschungsgemeinschaft through the Graduate College "Modern Methods of Magnetic Resonance in Materials Science". The authors wish to thank Maximilian Fichtner, Christoph Frommen and Wiebke Lohstroh from the Karlsruhe Research Center, Karlsruhe, Germany, for their help with the sample preparation. Thanks are due to Ivan Halasz for kindly providing the numerical values of the interatomic distances for the different configurations, obtained by using the program "Diamond, Crystal Impact, 2008". The authors are also grateful to Lothar Schimmele and Rainer Kimmich for valuable discussions of many theoretical aspects of the work.

References

[1] B. Bogdanović, M. Schwickardi, J. Alloys Compd. 253–254 (1997) 1.
[2] B. Bogdanović, R.A. Brand, A. Marjanović, M. Schwickardi, J. Tölle, J. Alloys Compd. 302 (2000) 36.
[3] R.A. Zidan, S. Takara, A.G. Hee, C.M. Jensen, J. Alloys Compd. 285 (1999) 119.
[4] C.M. Jensen, K.J. Gross, Appl. Phys. A 72 (2001) 213.
[5] K.J. Gross, G.J. Thomas, C.M. Jensen, J. Alloys Compd. 330–332 (2002) 683.
[6] A. Zaluska, L. Zaluski, J.O. Ström-Olsen, J. Alloys Compd. 298 (2000) 125.
[7] D.L. Anton, J. Alloys Compd. 356–357 (2003) 400.
[8] B. Bogdanović, M. Felderhoff, S. Kaskel, A. Pommerin, K. Schlichte, F. Schüth, Adv. Mater. 15 (2003) 1012.

[9] M. Fichtner, O. Fuhr, O. Kircher, J. Rothe, Nanotechnology 14 (2003) 778.
[10] J.W. Lauher, D. Dougherty, P.J. Herley, Acta Cryst. B35 (1979) 1454.
[11] V.K. Bel'skii, B.M. Bulychev, A.V. Golubeva, Russ. J. Inorg. Chem. 28 (1983) 1528.
[12] B.C. Hauback, H.W. Brinks, C.M. Jensen, K. Murphy, A.J. Maeland, J. Alloys Compd. 358 (2003) 142.
[13] V. Ozolins, E.H. Majzoub, T.J. Udovic, J. Alloys Compd. 375 (2004) 1.
[14] P. Canton, M. Fichtner, C. Frommen, A. Léon, J. Phys. Chem. B 110 (2006) 3051.
[15] J. Senegas, M. Villepastour, B. Bonnetot, J. Phys. Chem. Solids 42 (1981) 1061.
[16] V.P. Tarasov, G.A. Kirakosyan, Russ. J. Inorg. Chem. 42 (1997) 1349.
[17] V.P. Balema, J.W. Wiench, K.W. Dennis, M. Pruski, V.K. Pecharsky, J. Alloys Compd. 329 (2001) 108.
[18] J.W. Wiench, V.P. Balema, V.K. Pecharsky, M. Pruski, J. Solid State Chem. 177 (2004) 648.
[19] G. Majer, E. Stanik, L.E. Valiente-Banuet, F. Grinberg, O. Kircher, M. Fichtner, J. Alloys Compd. 404–406 (2005) 738.
[20] B. Bogdanović, M. Felderhoff, M. Germann, M. Härtel, A. Pommerin, F. Schüth, C. Weidenthaler, B. Zibrowius, J. Alloys Compd. 350 (2003) 246.
[21] J.L. Herberg, R.S. Maxwell, E.H. Majzoub, J. Alloys Compd. 417 (2006) 39.
[22] J.H. van Vleck, Phys. Rev. 74 (1948) 1168–1183.
[23] W.-K. Rhim, A. Pines, J.S. Waugh, Phys. Rev. Lett. 25 (1970) 218.
[24] W.-K. Rhim, A. Pines, J.S. Waugh, Phys. Rev. B 3 (1971) 684.
[25] A. Pines, W.-K. Rhim, J.S. Waugh, J. Magn. Res. 6 (1972) 457.
[26] H. Schneider, H. Schmiedel, Phys. Lett. 30A (1969) 298.
[27] H. Schmiedel, H. Schneider, Ann. Phys. 32 (1975) 249.
[28] R.C. Bowman Jr., W.-K. Rhim, J. Magn. Res. 49 (1982) 93.
[29] S.K. Brady, M.S. Conradi, G. Majer, R.G. Barnes, Phys. Rev. B 72 (2005) 214111.
[30] K. Takegoshi, D.A. McDowell, Chem. Phys. Lett. 116 (1985) 100.
[31] S. Hafner, D.E. Demco, R. Kimmich, Solid State Nucl. Magn. Reson. 6 (1996) 275.
[32] R. Kimmich, NMR Tomography, Diffusometry, Relaxometry, Springer, Berlin, 1997.
[33] E.L. Hahn, Phys. Rev. 80 (1959) 580.
[34] S. Matsui, Chem. Phys. Lett. 179 (1991) 187.
[35] I.J. Lowe, R.E. Norberg, Phys. Rev. 107 (1957) 46.
[36] T. Schobe, H. Wenzl, in: G. Alefeld, J. Völkl (Eds.), Hydrogen in Metals II, Springer, Berlin, 1978, p. 11.